The utilization of waste cooking palm oil as a green carbon source for the growth of multilayer graphene

M. F. Malek, M. Robaiah, A. B. Suriani, M. H. Mamat, M. K. Ahmad, T. Soga, M. Rusop, S. Abdullah, Z. Khusaimi, M. Aslam & N. A. Asli

Journal of the Australian Ceramic Society

ISSN 2510-1560

J Aust Ceram Soc
DOI 10.1007/s41779-020-00539-0

Springer

Journal of the Australian Ceramic Society
https://doi.org/10.1007/s41779-020-00539-0

RESEARCH

The utilization of waste cooking palm oil as a green carbon source for the growth of multilayer graphene

M. F. Malek[1,2] · M. Robaiah[1,2] · A. B. Suriani[3,4] · M. H. Mamat[5] · M. K. Ahmad[6] · T. Soga[7] · M. Rusop[1,5] · S. Abdullah[1,2] · Z. Khusaimi[1,2] · M. Aslam[1,2] · N. A. Asli[1,2]

Received: 18 March 2019 / Revised: 7 October 2020 / Accepted: 18 November 2020

Abstract

Waste cooking palm oil (WCPO) has been utilized as a green carbon source for the synthesization of graphene by double thermal chemical vapor deposition. The WCPO was placed in the first furnace (precursor furnace) whereas nickel was placed in the second furnace (deposition furnace). The deposition temperatures were varied between 850 and 1100 °C. Raman results reveal the highest 2-D peak for the sample synthesized at 1000 °C, which indicates the high-quality formation of graphene. Besides, the sample also shows good crystallinity with a sharp peak at 26.8° which represents the hexagonal graphite structure and the introduction of graphene sheet formation. On the other hand, the FESEM image displays hexagonal structures since the graphene layers were formed after the precipitation of the carbon. Meanwhile, the UV-Vis result shows the highest reflectance in the visible light region which indicates the presence of the graphene layer on Ni.

Keywords Palm oil · Graphene · Nickel · Multilayer · Carbon

Introduction

Decades ago, rapid development of large-area and high-quality graphene to enhance the performance of electronics and optoelectronic devices has been investigated. In the meantime, the graphenes are capable candidates that can be fabricated in large quantities with low-cost with respect to existing carbon nanotubes [1–3]. Graphene is a two-dimensional material with a special band structure that has received tremendous attention due to its extraordinary properties and enormous potential for various applications like large specific surface area, ultrafast carrier mobility, mechanical flexibility, high thermal conductivity, optical transparency, etc. [4]. Various research groups have reported on the preparation of graphene using various carbon precursors such as methane, acetylene, benzene, xylene, toluene, etc. However, these carbon precursors are related to fossil fuels and might cause problems in terms of scarcity of resources in the future. Therefore, it is crucial to develop graphene using green sources and cheap materials as alternatives especially for big-scale production. Some research groups have synthesized graphene with the help of some metal catalysts using natural and waste hydrocarbon source precursors such as camphor, sesame oil, palm oil, tea tree extract, and solid plastic waste.

✉ M. F. Malek
mfmalek07@uitm.edu.my; mfmalek07@gmail.com

[1] NANO-SciTech Lab (NST), Centre for Functional Materials and Nanotechnology (FMN), Institute of Science (IOS), Universiti Teknologi MARA (UiTM), 40450 Shah Alam, Selangor, Malaysia

[2] Faculty of Applied Sciences, Universiti Teknologi MARA (UiTM), 40450 Shah Alam, Selangor, Malaysia

[3] Nanotechnology Research Centre, Faculty of Science and Mathematics, Universiti Pendidikan Sultan Idris (UPSI), 35900 Tanjung Malim, Perak, Malaysia

[4] Department of Physics, Faculty of Science and Mathematics, Universiti Pendidikan Sultan Idris (UPSI), 35900 Tanjung Malim, Perak, Malaysia

[5] NANO-ElecTronic Centre (NET), Faculty of Electrical Engineering, Universiti Teknologi MARA (UiTM), 40450 Shah Alam, Selangor, Malaysia

[6] Microelectronics and Nanotechnology - Shamsuddin Research Centre (MiNT-SRC), Faculty of Electrical and Electronic Engineering, Universiti Tun Hussein Onn Malaysia (UTHM), 86400 Parit Raja, Batu Pahat, Johor, Malaysia

[7] Department of Frontier Materials, Nagoya Institute of Technology (NITech), Gokiso-cho, Showa-ku, Nagoya, Aichi 466-8555, Japan

Published online: 24 November 2020

Sharma et al. synthesized a single-layer and bilayer graphene on nickel foil using solid camphor as a carbon source by the chemical vapor deposition (CVD) process in hydrogen and argon gas atmosphere [5]. They reported that the graphene layers grown with the mixture of Ar/H_2 gas show a larger size compared with those grown with single Ar gas. Besides, they also confirmed that the annealing process of Ni enhances the properties of graphene due to better coordination of segregated carbon from camphor. Sesame oil is another carbon source extracted from sesame seeds that has been used by Kumar et al. to produce graphene on SiO_2 substrate by the spray pyrolysis technique [6]. The as-synthesized graphenes show the formation of 6–8 layers of GNSs with no more functional group attached on the surface as confirmed with the FTIR spectra. They also reported that the growth of graphene is dependent on the temperatures inside the tube. On the other hand, Salifairus et al. was successfully synthesizing few layers of graphene by the CVD method using commercial palm oil from the existing market as a carbon source [7]. They studied the growth of graphene at deposition temperatures between 800 and 1100 °C. They optimized their sample at 900 °C and found that this parameter plays an important role to obtain a good quality of graphene. On the other side, Jacob et al. had successfully produced high-quality graphene films on silicon substrates using an extract from tea tree plant by the low-cost simple plasma-assisted CVD method without any catalyst [8]. This vertically oriented graphene has a high surface area and long edges provide unique functionalities. However, no significant changes were observed on the graphene beyond 4 min of the deposition process. Nonetheless, Sharma et al. synthesized a high-quality single-crystal graphene on Cu foil using solid waste plastic by the CVD method under Ar/H_2 gas at the temperature of 1020 °C [9]. The graphenes are uniformly distributed all over the Cu foil with a size of 100 μm and increase with the growth time. Besides, they reported that the growth of single-crystal graphene is strongly influenced by the injection rate of decomposed polymeric components generated during pyrolysis of plastic waste. On the other hand, the bilayer graphene crystals were produced at higher injection rate.

Palm oil, referred to as the oil extracted from the fruits of the oil palm tree (*Elaeis guineensis jacq.*), is edible plant oil that is naturally reddish as it contains high amounts of beta-carotene [10]. In Malaysia, palm oil has been usually used as cooking oil compared with other oils (canola oil, peanut oil, sunflower oil, soybean oil, olive oil) [11]. The palm oil production in this country has reached 5.0 million tonnes in 1980 and the market demand has increased up to 11.0 million tonnes which is greater than 50% compared with previous decades. The number has kept growing to 21.8 millions tonnes by the year 2000 [12]. Malaysia has produced 17.7 million tonnes on 4.5 million hectares of land, thus making Malaysia the second-largest producer and exporter of palm oil in the world after Indonesia during this period [13]. However, "waste cooking palm oil" (WCPO) is one of the pollutions that affect the aquatic life where it is normally discharged into the river system. WCPO refers to re-used oil which is commonly just thrown away or no longer viable for its intended use. The disposal of WCPO is quite challenging due to their physical form, which exists in a semi-liquid or semi-solid form. Usually, most people will just pour the waste into the kitchen sink, drain, and watercourse [14]. In an effort to make this material benefical, a process called transesterification was applied on the WCPO to produce a biodiesel. The optimum conditions for biodiesel production (oils/methanol ratio and concentration of catalyst) are inconsistent which strongly depend on the properties of WCPO [15]. The most common way to produce biodiesel is by transesterification which refers to a catalyzed chemical reaction involving triacylglycerol and an alcohol, usually methanol, in the presence of a catalyst such as potassium hydroxide (KOH) or sodium hydroxide (NaOH). This reaction will transform the triacylglycerol to yield fatty acid alkyl esters which is the biodiesel and glycerine which is shown in Fig. 1 [16].

In the meantime, the use of WCPO will be economically, environmentally beneficial and help to decrease human dependence on non-renewable petroleum energy sources. Lapuerta et al. discovered that the WCPO has a high carbon content which is 76.95% compared with refined palm oil (68.81%) [17]. Palmitic acid is a major component of palm oil with a chemical formula of $C_{16}H_{32}O_2$ and possesses 16 carbons in one chain. Meanwhile, the carbon content emerges as the main component atom supply for graphene synthesis [18]. According to Meesuk and Seammai, palmitic acid content that is present in used cooking palm oil is 6% higher compared with unused cooking palm oil [19]. The hydrocarbon chain of waste cooking palm oil molecules that is

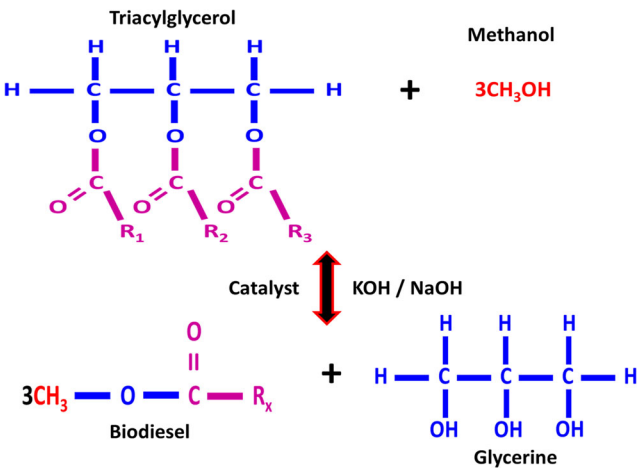

Fig. 1 Transesterification of triacylglycerol to yield biodiesel and glycerine

decomposed into smaller and lighter hydrocarbon is shown in Eq. (1) below:

$$C_{55}H_{100}O_6 + H_2O \rightarrow CO + CO_2 + C_xH_y + C_xH_yO_z + H_2O + OH^{\bullet} \quad (1)$$

where $x, y, z > 1$. Our main motivation in this paper is to utilize the waste carbon source product as "green" alternatives and cheap raw materials which is favorable for industrial-scale production. In this experiment, graphene was successfully synthesized using WCPO by the double thermal chemical vapor deposition (DTCVD) process on nickel (Ni) substrate at various deposition temperatures.

Experimental procedure

WCPO was obtained from refined domestic cooking palm oil that has been used to fry chickens. Each frying cycle lasted about 18 min at temperatures not exceed 180 °C. The oil is constantly used until three frying cycles with the same amount of chickens, time, and temperatures. It is knowledgeable that graphene is made of pure carbon; hence, the WCPO was used as the carbon source. The WCPO was filtered using the filter funnel and filter paper to remove solid objects and precipitate. Meanwhile, the substrate was prepared by cutting the Ni foil into an area of 1 cm^2; cleaned with acetone, ethanol, methanol, and deionized water; and finally dried. DTCVD was used to synthesize graphene. An alumina boat containing waste cooking palm oil was placed at a distance of 15 cm from the center point of the tube in the first furnace. Ni substrate was placed on the alumina boat at a distance of 15 cm from the center point of the tube in the second furnace. Argon gas was flown for 10 min at 200 sccm to flush out any impurities inside the quartz tube and to give an inert atmosphere for the deposition purpose. The temperature of the precursor was fixed to 350 °C and the deposition temperatures varied from 850 to 1100 °C. The synthesis process took 15 min and then the sample was cooled down to ambient temperature. Based on the accepted growth mechanism on Ni, graphene was formed on the Ni surface as a result of the segregation and precipitation of the carbon atoms on the substrate during cooling. The corresponding process is shown in Fig. 2. The Raman spectra were measured using Raman spectroscopy with Ar laser operating at 514 nm as the excitation source (Horiba Jobin Yvon-79DU420A-OE-325) to detect the graphene since it is very sensitive to geometric structure and bonding within molecules for different allotropes of carbon. The crystal structure properties and phases of the prepared graphenes were investigated by using an X-ray diffractometer (XRD; Shimadzu-6000) with Cu-Kα radiation, $\lambda = 1.5405$. The beam voltage and beam current were 30 kV and 20 mA, respectively. The morphological properties and composition analysis were investigated by field emission scanning electron microscopy (FESEM; JEOL JSM-7600F) while the surface topography, hexagonal pattern, and uniformity of grown graphene were examined by atomic force microscopy (AFM; XE-100 Park System). On the other hand, the optical measurements of the samples were carried out using a UV-visible-near-infrared spectrophotometer (UV-Vis-NIR; Varian Cary 5000) within the range from 200 to 800 nm at room temperature to determine the structure of the sp^2- and sp^3-hybridized carbon atoms.

Results and discussion

Raman spectra and analysis of the graphene film were shown in Fig. 3 and Table 1. The graph shows the informative Raman bands of graphene are in the range from 500 to 3000 cm^{-1}. The Raman spectrum of graphene is known to be very sensitive to the number of atomic layers and degree of structural disorder or defects [20]. All the spectra show the three major Raman peaks for graphene, which are the D, G, and 2-D peaks. The D peak is located at around 1350 cm^{-1} that is caused by a disorder in sp^2-hybridized structure of graphene.

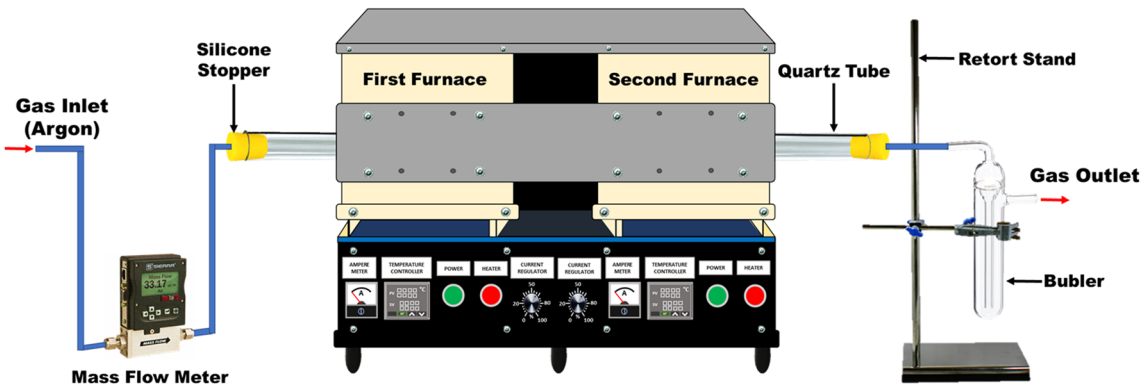

Fig. 2 Schematic diagram of graphene preparation at different temperatures

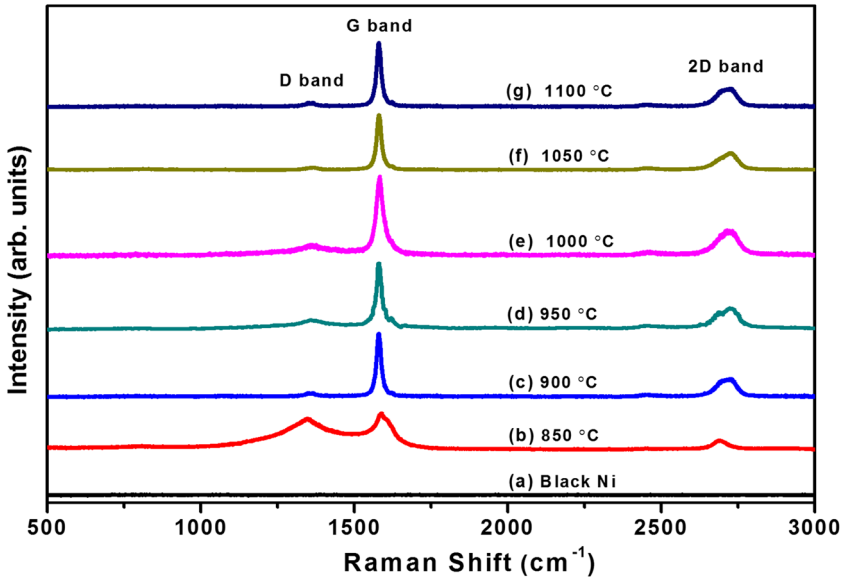

Fig. 3 Raman analysis of graphene at different deposition temperatures (**a**) blank Ni, (**b**) 850, (**c**) 900, (d) 950, (**e**) 1000, (**f**) 1050, and (**g**) 1100 °C

The presence of disorder in sp^2-hybridized structure results in resonance Raman spectra. Meanwhile, the G peak which is located at about ~ 1583 cm^{-1} is due to E_{2g} symmetry phonons at the center of the Brillouin zone (Γ-point). The G peak arises from the C–C bond stretch which highly sensitive to strain effects in the sp^2 system, and thus can be used to probe modification on the flat surface of graphene [21].

As shown in Fig. 3(b), the D band is seen at ~ 1347 cm^{-1} and the G band at ~ 1589 cm^{-1}. The D band is quite intense and broader because of the higher level of disorder of the graphene layers [22]. These happened due to the oxygenation of graphite, which results in the formation of sp^3 carbon atoms. Besides, the D band in the graphene layer is broadened as a result of the degradation of in-plane sp^2, reduction in the size of the sp^2 domains by the creation of defect, vacancies, and distortions during oxidation [23]. The D to G band intensity ratio of I_D/I_G helps in determining the defect density in the graphene films [20]. It reveals that the D and G bands of graphite are sharper and more intense as the deposition temperature increases up to 1000 °C [24]. After that, both the D band and G band is shifted to a lower intensity. As the temperature rises, the intensity of I_D/I_G is clearly decreasing with the increment in deposition temperature. This indicated a better formation of graphene and reduction of defects.

In the meantime, the second-order band occurring between 2500 and 2800 cm^{-1} has been referred to as double resonance which is the 2-D peak. The shape of the 2-D band and the ratio of I_{2D}/I_G is an important parameter to identify the number of atomic graphene layers, n from $n = 1$ to approximately $n = 7$ [25]. The presence of the 2-D peak in the Raman spectra of graphene is sensitive to the number of graphene atomic layers. The ratio I_{2D}/I_G of the intensity of the bands 2D and G is dependent on the number of graphene layers [26, 27]. The ratio $I_{2D}/I_G \sim 2$–3 is for monolayer graphene, $2 > I_{2D}/I_G > 1$ for bilayer graphene and $I_{2D}/I_G < 1$ for a multilayer one. Based on the ratio I_{2D}/I_G of Raman spectra, it can be concluded that the graphene films grown on the Ni foil are multilayers. Besides, the less intense and broad 2-D peak confirmed the formation of multilayer graphene [25]. The graphene films grown at 1000 °C have a higher ratio I_{2D}/I_G compared with

Table 1 Raman peaks of the graphene layer at different deposition temperatures

Sample	D band		G band		2D band		I_D/I_G	I_{2D}/I_G
	Position (cm^{-1})	Height	Position (cm^{-1})	Height	Position (cm^{-1})	Height		
(a) Blank Ni	–	–	–	–	–	–	–	–
(b) 850 °C	1347	259.17	1589	294.96	2690	101.06	0.88	0.34
(c) 900 °C	1353	28.65	1581	449.28	2721	124.42	0.06	0.28
(d) 950 °C	1356	81.67	1582	479.37	2724	164.05	0.17	0.34
(e) 1000 °C	1357	89.64	1583	552.76	2724	192.59	0.16	0.35
(f) 1050 °C	1363	21.99	1581	389.23	2724	121.06	0.05	0.31
(g) 1100 °C	1362	23.32	1581	449.28	2724	124.42	0.05	0.28

other graphene films. These results show that the DTCVD temperature of 1000 °C is the optimum temperature for growing good-quality graphene films on the Ni foil surface. As the deposition process reaches an optimum temperature, the G band tends to become narrow and symmetric. This result reflects an optimum temperature for carbon giving rise to relatively good crystallinity. However, the presence of the defect still exists at 1000 °C due to the non-sp^2 bond formation of C atoms. At higher growth temperatures, the reconstruction of Ni grain boundaries occurs and hence created a rough surface, which is expected to contribute to the formation of multilayer graphene and small graphite crystallite [28]. It was found that the number of graphene layers is sensitive to the growth temperature. The polycrystalline Ni leads to a higher percentage of multilayer graphene due to the presence of grain boundaries. For example, Lee et al. observed that the grain boundaries can be the nucleation sites for multilayer graphene growth [29].

The XRD pattern in Fig. 4 showed good agreement with the crystalline phases (fcc) according to the alloy composition. The peaks at 44.4, 54.5, and 77.2° show the pure Ni phase corresponding to (111), (200), and (220) crystal planes that match the patterns [JCDPS No. 00-001-1266]. In addition, the peak at 26.4° corresponds to the diffraction peaks of graphitic structure [JCPDS No. 41-1487] [30]. As can be seen, the observed XRD peaks at sample Fig. 4a indicate the presence of Ni phase whereby no graphite phases have been detected. Meanwhile, Fig. 4b shows a very low-intensity peak that appeared around 26.8° which indicates the distorted graphite structure, thus suggesting the introduction of the formation of graphene sheet [31]. At the lowest deposition temperature, the nucleation process occurred slowly which unfavorably

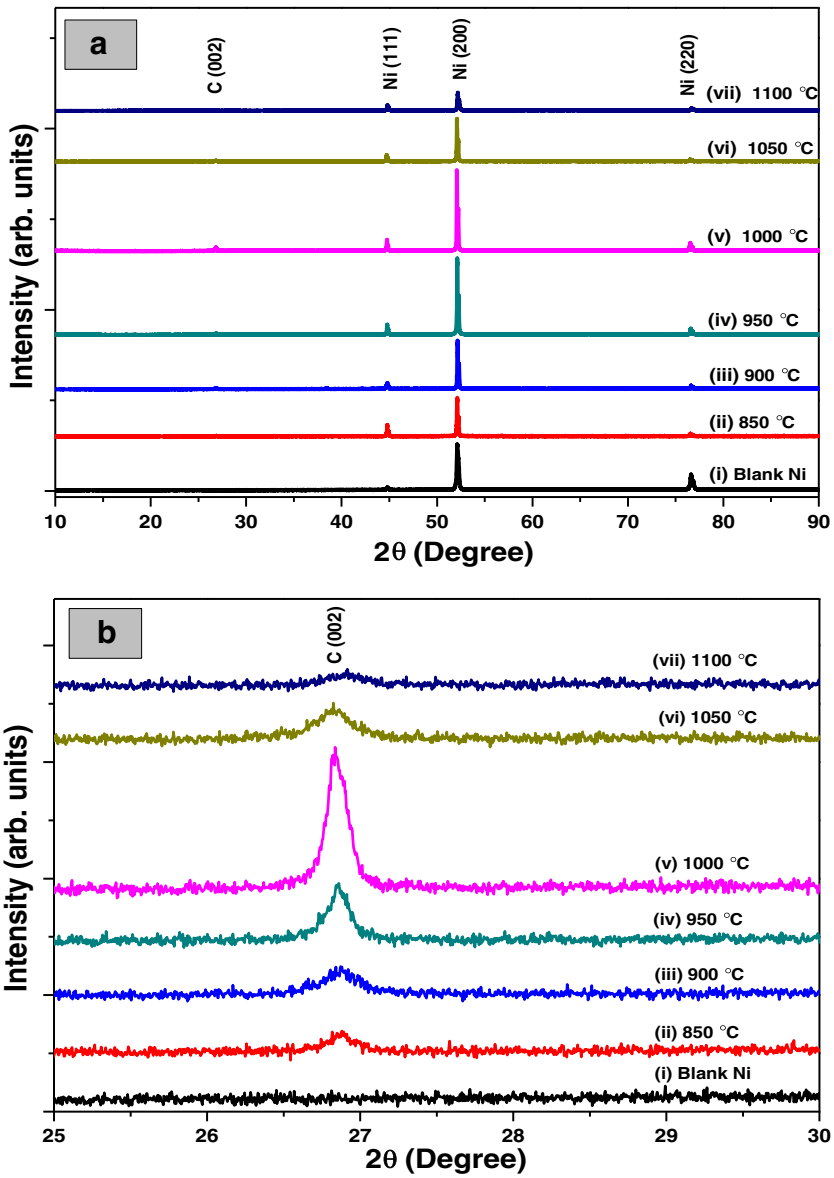

Fig. 4 XRD patterns of graphene from **a** 10–90° and **b** 25–30° at different deposition temperatures

creates less Ni nucleation sites for graphene to incorporate into the Ni matrix. On the other hand, increasing the graphene/carbon apparently increased the peak intensity of (002) due to the increment of the deposition temperature [32]. As shown in the diffractogram, the sample at 1000 °C of deposition temperature possesses good crystallinity with a sharp peak at 26.8° which represents the characteristic peak of the (002) plane in hexagonal graphite [33]. The peak (002) observed at $2\theta = 26.8°$ corresponds to the d-spacing of about 0.34 nm which is associated with a good arrangement of the interlayer distance of graphene as reported by previous studies [34, 35]. A small peak in the 2θ range of 20–30° arose due to the C (002) peak present in graphene which indicates a short-range order of the carbon atoms as claimed by Vinayan et al. [36]. At this temperature, the peak intensity gradually increased due to the rapid reduction of Ni ions and increment of the nucleation orientations on both (111) and (200) planes [32]. The peak intensity of (200) is notably higher than (111) with the introduction of graphene onto the Ni deposition process as it might alter the pattern of preferred orientations, crystal orientation, and growth behavior [37]. Further extending the deposition temperature beyond an optimum temperature has resulted in the disappearance peak at 26.8° as observed in Fig. 4b (v, vi) which indicates decrement of grain size and surface roughness with low intensity of graphene. In fact, Ni reduction occurred rapidly under higher temperature conditions leading to the agglomeration of graphene and less aggregate of graphene notably engulfed/penetrated into the Ni matrix [32].

The surface morphology of deposited graphene was observed by FESEM in Fig. 5 with a magnification of 5 k at different deposition temperatures. Figure 5a represents the surface morphology of blank Ni foil. As can be seen, the

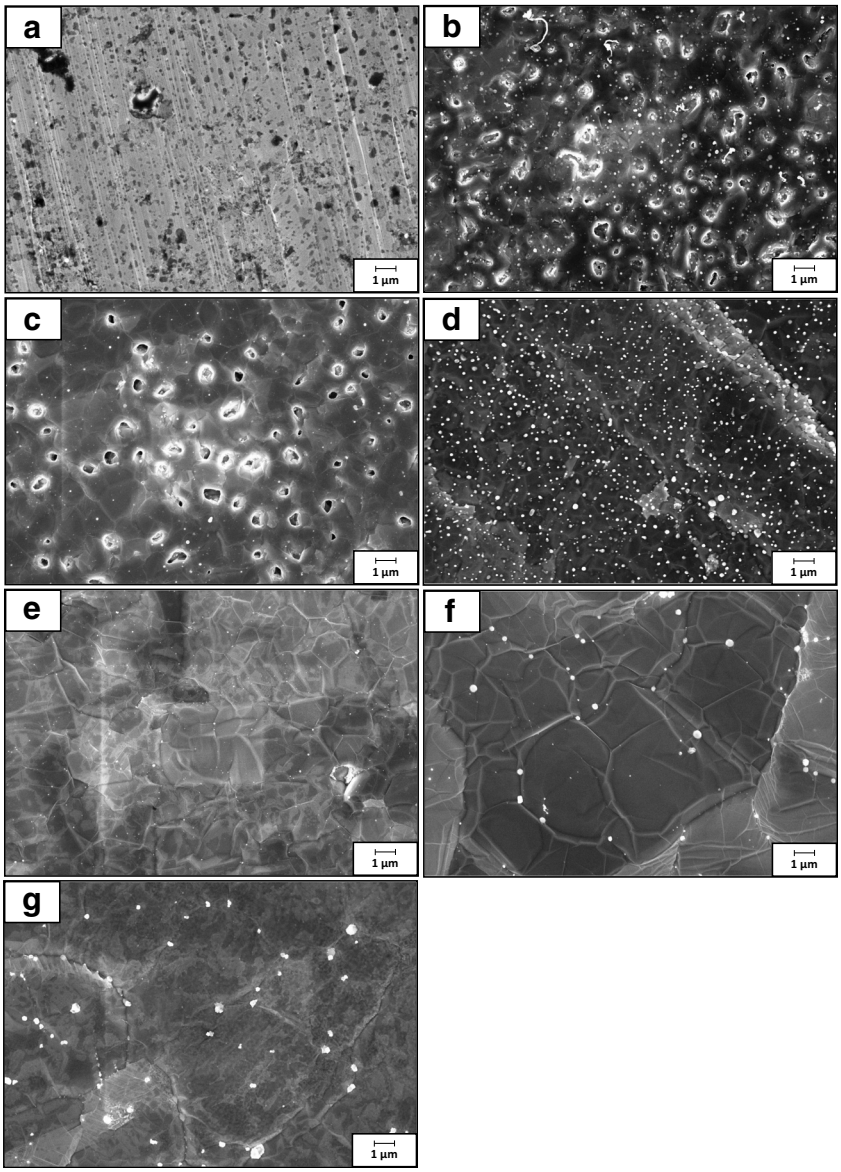

Fig. 5 FESEM images of graphene at different deposition temperatures **a** blank Ni, **b** 850, **c** 900, **d** 950, **e** 1000, **f** 1050, and **g** 1100 °C

deposition temperature has a significant effect on the surface morphologies of graphene. In Fig. 5b, the film which is deposited at 850 °C showed the dark fragments and wrinkles are graphitic-like carbon fragments [38]. This phenomenon could have resulted from the segregation of C_2H_2 being too quick, hence reduced the carbon particle covered the Ni surface. The image revealed in Fig. 5c demonstrates hexagonal shapes that are not perfectly grown with larger bright particles which are considered porous structures on the surface of the sample. This phenomenon occurs due to low segregations of carbon atom on the Ni surface and when no in situ hydrogen plasma posttreatment is performed [20]. The experimental results show that the increase in deposition temperature up to 950 °C produces thinner multilayer graphene on transition metals. At this temperature, the wrinkles and coarser, compact, and hexagonal shapes were found within the multilayer graphene, resulting in dislocation and distortion. Moreover, the multilayer graphene is not ideally smooth, which might be caused by the crack phenomenon during the growth process. Zhang and Feng had emphasized that keeping the increase in the substrate temperature probably would result in the good quality of graphene [39]. At the optimum deposition

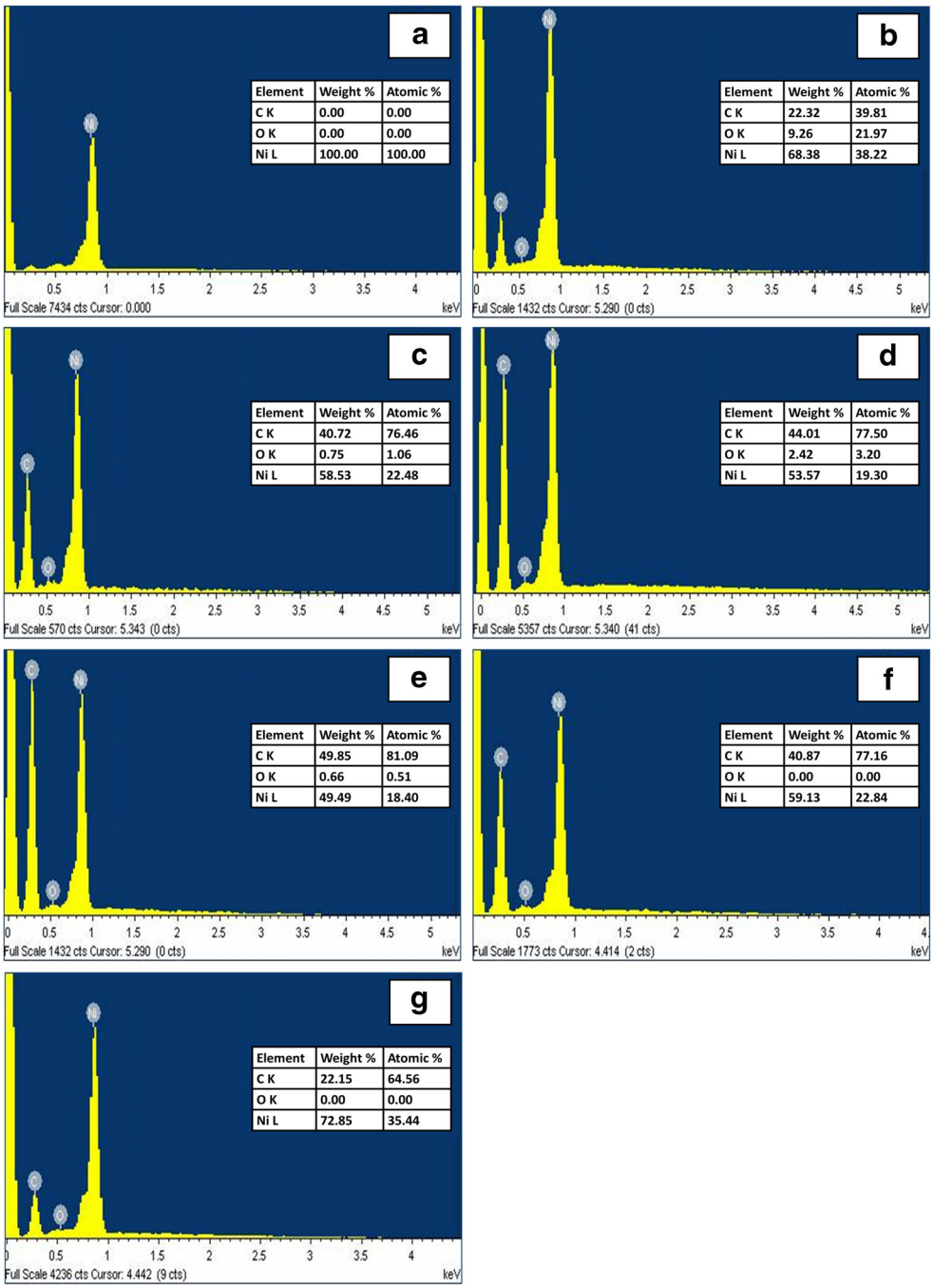

Fig. 6 EDX analysis of graphene at different deposition temperatures **a** blank Ni, **b** 850, **c** 900, **d** 950, **e** 1000, **f** 1050, and **g** 1100 °C

temperature as shown in Fig. 5e, hexagonal-like shapes were formed indicating the formation of graphene layers after segregation of carbon atom on the Ni surface, which would clarify the precipitation phenomenon [38]. It can be observed that the carbon atoms accumulate along the grain boundaries, which represent the high curvature and high density of atomic steps at the boundaries [40]. Besides, the visible wrinkles and folding effect that were observed might be related to the stress release from the deviation of the thermal expansion coefficients between the Ni and graphene [41]. Besides, the formation of wrinkles is attributed to the slow diffusion rate of the carbon atom through the grain boundary. An interesting feature to be highlighted is that the wrinkle density decreased as the deposition temperature increase beyond the optimum temperature [35]. The analysis from the grain boundaries after graphene growth reveals the nucleation sites are multilayer graphene. The rise in deposition temperature leads to the change of shapes and different densities as shown in Fig. 5f.

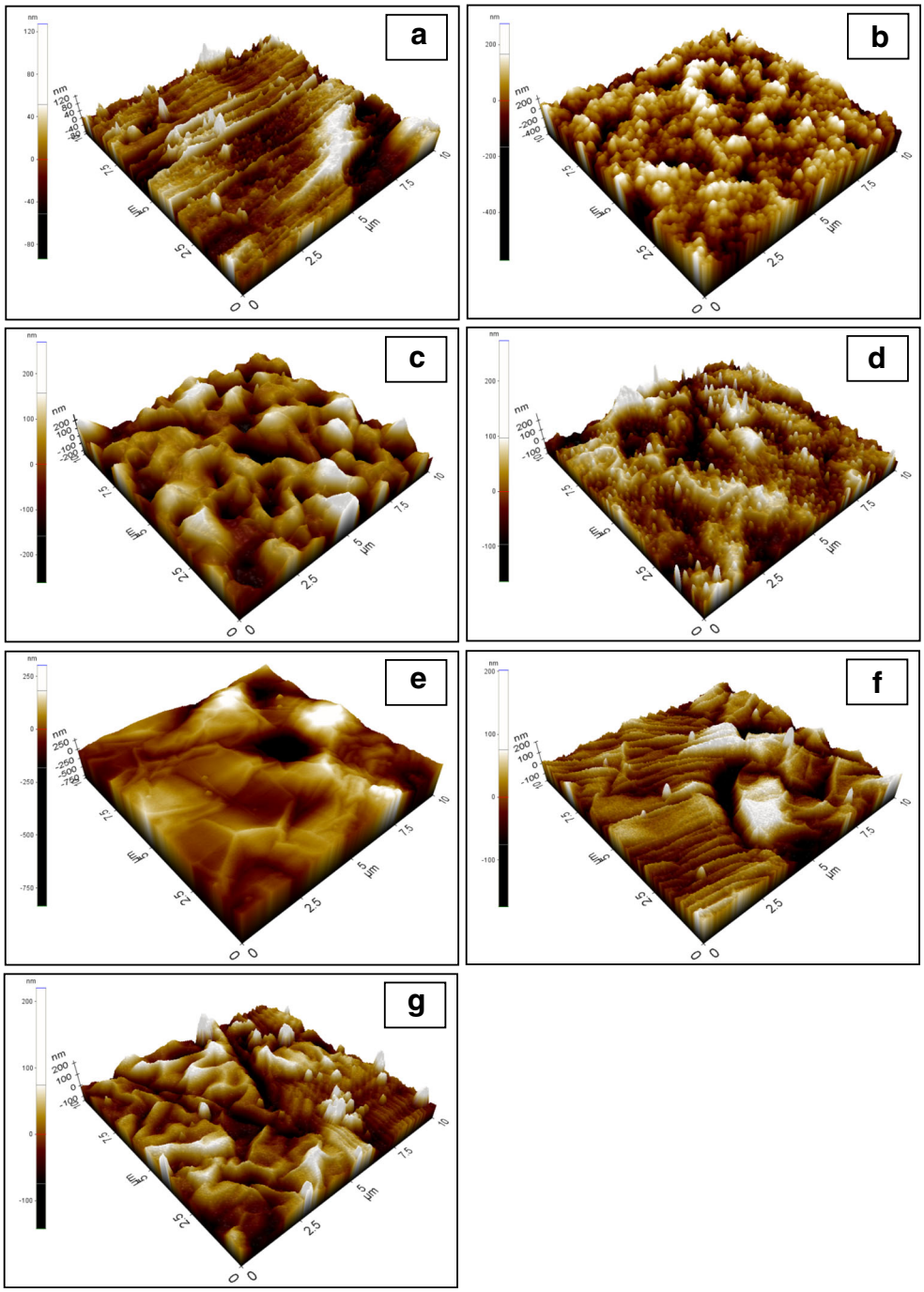

Fig. 7 AFM tophography of graphene at different deposition temperatures **a** blank Ni, **b** 850, **c** 900, **d** 950, **e** 1000, **f** 1050, and **g** 1100 °C

Table 2 Average roughness topography of graphene layer at different deposition temperatures

Samples	Deposition temperature (°C)	Roughness (nm)	Standard error
(a)	Blank Ni	20.099	–
(b)	850	67.507	0.553
(c)	900	63.292	0.442
(d)	950	54.084	0.315
(e)	1000	49.275	0.197
(f)	1050	28.859	0.225
(g)	1100	29.601	0.478

Meanwhile, with further increase in deposition temperature above 1000 °C, the samples tend to degrade and being more compact as shown in Fig. 5g. This is correlated to some voids and cracks appeared on the surface. The quality and quantity of graphene are strongly influenced by the deposition temperature. Consequently, it should be noted that the growth temperature is one of the fundamental core to be considered for graphene formation.

The energy-dispersive X-ray (EDX) spectrum of graphene film is shown in Fig. 6. The EDX spectrum shows the appearance of carbon, oxygen, and nickel with different weight percentages. The appearance of these peaks in the EDX measurement confirmed the existence of NiO and graphene [42]. In addition, the presence of Ni and C which certify the incorporation of graphene in the nickel matrix during the deposition process [32]. The EDX analysis in Fig. 6a shows the sample consist of nickel element only with weight percentages 100%. The EDX analysis from Fig. 6b revealed that the composition in the films consisted of carbon, oxygen and nickel are 22.32, 9.26, and 68.38 wt% respectively. Figure 6 c–e shows the increment of carbon weight percentage by increasing deposition temperature reach to the optimum. Stefanos Chaitoglou and Enric Bertran revealed that lower nucleation and higher growth rates can be achieved by varying the growth temperature at optimum condition [43]. The changes of oxygen peaks qualitatively in EDX peaks confirm the low oxygen content of the graphene films. This phenomenon could result from the high degree of reduction of GO by increasing the growth temperature [44]. More interestingly, the control of the growth temperature influenced the segregation of the carbon atoms on the surface and forms six-atom rings. Upon the EDX results, it is clearly proven that higher growth temperature will eliminate the oxygen from the graphene [22]. At an optimum growth temperature, the percentage of carbon atoms is highest which is 49.75 wt% compared with other samples which are considered excellent anchoring sites for metal nanoparticles [41]. In contrast, increasing the deposition temperature above the optimum point can result in the loss of oxygen atoms and decrease the weight percent of carbon atoms as shown in Fig. 6f, g. Besides, some defects can be generated during the synthesis process on the Ni surface at a higher temperature [45]. It can be concluded that the increase in deposition temperature may result in low energies for hydrocarbon adsorption and decrease the amount of carbon atom diffusion, thus allowing multilayer graphene formation [46].

Figure 7 shows the level of exfoliation evaluated by AFM at various deposition temperatures. Apparently, the surface of Ni (111) shows a smooth appearance with almost no grain boundaries corresponding to the non-introduction of carbon source as depicted in Fig. 7a. The AFM results showed the average surface roughness changed from 67.507 to 29.601 nm with a deposition temperature from 850 to 1100 °C respectively. Figure 7 b shows the graphene started to nucleate and agglomerate where the graphene is bonded to the diamond. The size of graphene crystals

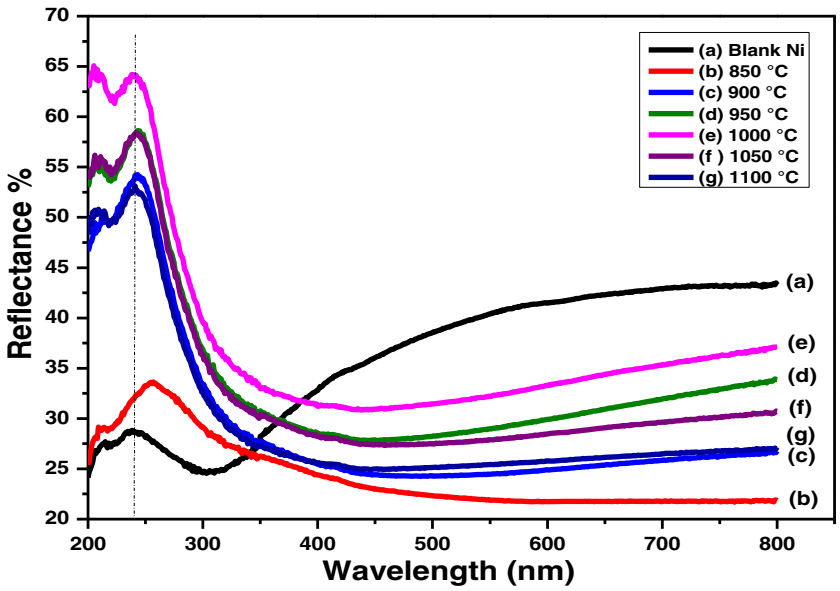

Fig. 8 UV-Visible spectrum results of graphene at different deposition temperatures **a** blank Ni, **b** 850, **c** 900, **d** 950, **e** 1000, **f** 1050, and **g** 1100 °C

increases significantly with temperature, as the temperature increases to 900 °C, the particle start to form coalescence and hexagonal structure. Meanwhile, the sample in Fig. 7c shows the topography of the underlying substrate with slightly decreased roughness. On the other hand, the graphene grain was growing larger at 1000 °C. The grain size further increases when it breaks the thermodynamic equilibrium of graphene growth. As shown in Fig. 7d, it is clear that the process of increasing synthesis temperature can yield continuous growth of graphene grains. The continuous increase in the temperature reached the optimum Fig. 7e and increased the density of active carbon-related radicals on Ni and breaks the dynamic equilibrium at graphene edges. Thus, this process results in continuous graphene growth [47]. Moreover, at this temperature, the carbon lattice in graphene has strong and highly directional bonds. The segregation of carbon atoms produces few layers of graphene on the top of the surface. The final thickness of graphene is related to the amount of dissolved carbon into nickel and the diffusion and final segregation, as well as nucleation on the surface [48]. In contrast, for AFM images at a higher temperature (Fig. 7 f and g), the samples revealed the topological defects between the two commensurate phases that are called solitons and domain walls. These probably might be due to molecular structures that store the "strain" imposed on the graphene layer of the nickel substrate/graphene structure [49]. The change of roughness attributed to the grain boundary between graphene and nickel substrate [50]. By controlling the surface roughness of the nickel substrate, it can result in the tunable adhesion of graphene [48]. The variation in average roughness is presented in Table 2. Hence, it is concluded that all these processes strongly depend on temperature.

The reflectance of graphene at various deposition temperatures was depicted in Fig. 8, which is important to indicate the formation of graphene on the Ni substrate. Figure 8 a shows the Ni foil substrate before the formation of graphene as a comparison. No obvious peak was observed at a wavelength of 230 nm. The percentages of reflectance at 850 °C show a weak peak which is 34% as a high shoulder at 250 nm. At this temperature, the shift of the UV peak occurred due to the hydrogenated amorphous carbon grains [51] and the graphene size growth. Through the AFM result, at this temperature, the graphene just started to agglomerate and not fully grown yet. The UV-Vis spectra reveal that the samples at different synthesis temperatures show a different reflectance percentage. As synthesis temperature increases, carbon reflected more excitation energy of carbon atom since graphene has transparency characteristics. In other words, the introduction of the high addition amount of graphene carbon atom led to shielding of the active sites on the catalyst surface and also rapidly increased the intensity of light reflected on the sample, which could be called a "shielding effect" [52]. Sample at 1000 °C showed an optimum reflectance in the entire visible light region. From the results, a peak around at a wavelength of 230 nm becomes suddenly obvious and sharpened. This phenomenon occurs when the sample was exposed to UV light where the atomic structure of the sample becomes excited. Hence, the excitation result is reflected and gathered in the form of a spectrum [53]. This kind of characteristic features was observed in these spectra to identify graphene. The characteristic feature appears at the shape of a peak at 230 nm and corresponds to π-π* plasmon peak [54]. In principle, the π-π* band position is a carbon-based material that is related to the sp^2/sp^3 character in which the growth of the graphene sp^2 layers occurs [55]. In contrast, the sample at high synthesis temperature showed a decrease in reflectance. According to Agorku et al., this is correlated to the bandgap excitation of the electron band to the conduction band [56]. Thus, it is revealed that the decrease in percentages of reflectance is caused by a conjugative effect related to chromosphere aggregation that influences the π-π* plasmon peak [53]. Any experiment will aim to obtain a high yield of

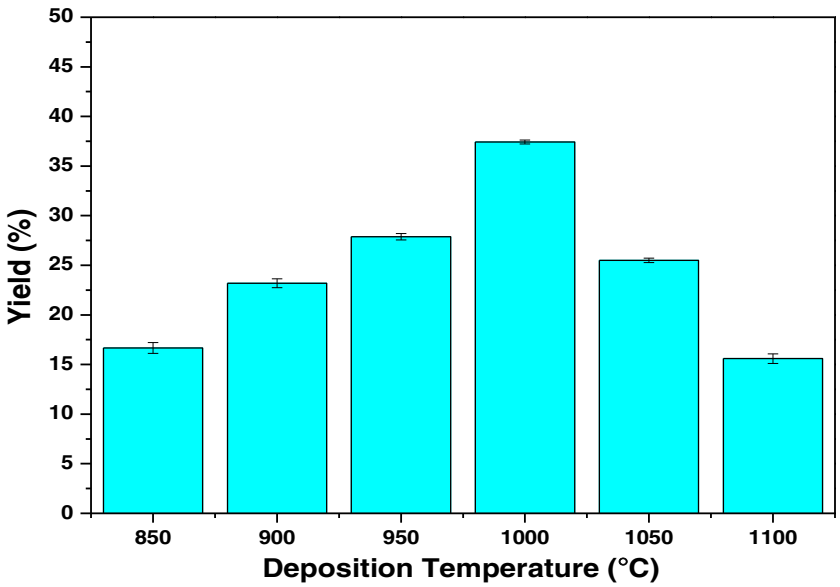

Fig. 9 Histograms of yield and standard error for graphene deposited at different temperatures

graphene. Thus, all samples were being run and repeated for few times in order to determine its quality and also to check the repeatability of the process. Figure 9 shows the average percent yield and standard deviation of the graphene growth at various deposition temperatures as tabulated in Table 2. The average percentage growth of the graphene is highest at 1000 °C of deposition temperature. Thus, the first interpretation from the data analysis in Table 2 explained that 1000 °C of deposition temperature could achieve good growth compared with others. The standard error of all runs was in the range of 0.197–0.553.

Conclusion

Multilayer graphene films were successfully synthesized on the Ni foil by the DTCVD method between 850 and 1100 °C. The structure and quality of the graphene films were improved with the increase in the deposition temperature. XRD analysis reveals the presence of a carbon peak (002) at 26.8° which indicated the existence of a smaller crystalline size of graphene in a few layer structures. By controlling the growth temperature at the optimum, AFM images at the temperature of 1000 °C form coalescence and hexagonal structure which indicated that the graphene layers were successfully established since the precipitation of carbon has been completed. Consequently, this study has successfully demonstrated that utilization of waste cooking palm oil as the carbon source for the fabrication of graphite is possible. This opens a promising way for application of graphene films in gas detectors and sensors. In the meantime, using these sources as a precursor can reduce the cost and consumption of limited fossil fuels.

Acknowledgments The authors thank Mrs. Ts. Irmaizatussyehdany Buniyamin (Senior Research Officer), Mr. Ts. Salifairus Mohammad Jafar (UiTM Senior Science Officer), Mr. Mohd Azlan Jaafar (UiTM assistant engineer), Mr. Suhaimi Ahmad (UiTM assistant engineer), and Mr. Muhamad Faizal Abd Halim (Assistant Research Officer) for their kind support on this research.

Funding This work was supported by Grant Nos. 600-IRMI/FRGS-RACER 5/3 (102/2019) and 600-RMIS/1/RAGS 5/3. The study also received financial support from the Research Management Centre (RMC), Universiti Teknologi MARA (UiTM), and the Ministry of Higher Education Ministry (MoHE), Malaysia.

References

1. Suriani, A.B., Nor, R., Rusop, M.: Vertically aligned carbon nanotubes synthesized from waste cooking palm oil. J Ceram Soc Japan. **118**, 963–968 (2010)
2. Tsai, T.-Y., Tai, N.-H., Chen, K.C., Lee, S.H., Chan, L.H., Chang, Y.Y.: Growth of vertically aligned carbon nanotubes on glass substrate at 450 °C through the thermal chemical vapor deposition method. Diam Relat Mater. **18**, 307–311 (2009)
3. Mittal, G., Dhand, V., Rhee, K.Y., Park, S.-J., Lee, W.R.: A review on carbon nanotubes and graphene as fillers in reinforced polymer nanocomposites. J Ind Eng Chem. **21**, 11–25 (2015)
4. K. Kanahashi, M. Ishihara, M. Hasegawa, H. Ohta and T. Takenobu, "Giant power factors in *p*- and *n*-type large-area graphene films on a flexible plastic substrate". *Npj 2D Mater. Appl.,* vol. 3, p. 44, 2019
5. Sharma, S., Kalita, G., Hirano, R., Hayashi, T., Tanemura, M.: Influence of gas composition on the formation of graphene domain synthesized from camphor. Mater Lett. **93**, 258–262 (2013)
6. Kumar, R., Singh, R.K., Kumar, P., Dubey, P.K., Tiwari, R.S., Srivastava, O.N.: Clean and efficient synthesis of graphene nanosheets and rectangular aligned-carbon nanotubes bundles using green botanical hydrocarbon precursor: sesame oil. Sci AdvMater. **6**, 76–83 (2014)
7. Salifairus, M.J., Hamid, S.B.A., Soga, T., Alrokayan, S.A.H., Khan, H.A., Rusop, M.: Structural and optical properties of graphene from green carbon source via thermal chemical vapor deposition. J Mater Res. **31**, 1947–1956 (2016)
8. Jacob, M.V., Rawat, R.S., Ouyang, B., Bazaka, K., Kumar, D.S., Taguchi, D.: Catalyst-free plasma enhanced growth of graphene from sustainable sources. Nano Lett. **15**, 5702–5708 (2015)
9. Sharma, S., Kalita, G., Hirano, R., Shinde, S.M., Papon, R., Ohtani, H.: Synthesis of graphene crystals from solid waste plastic by chemical vapor deposition. Carbon. **72**, 66–73 (2014)
10. Sanli, H., Canakci, M., Alptekin, E.: Characterization of waste frying oils obtained from different facilities. Bioenergy Technol. **8**, 479–485 (2011)
11. Mayne, M., Grobert, N., Terrones, M., Kamalakaran, R., Rühle, M., Kroto, H.W., Walton, D.R.M.: Pyrolytic production of aligned carbon nanotubes from homogeneously dispersed benzene-based aerosols. Chem Phys Lett. **338**, 101–107 (2001)
12. N. Abdullah and F. Sulaiman, "The oil palm wastes in Malaysia," in Biomass now: sustainable growth and use, 1st ed., InTech, Croatia, pp. 75–93, 2013
13. Zaharudin, R.R.N.A., Esivan, S.M.M., Othman, N., Idris, A.: Review on the potential use of waste cooking palm oil in the production of high oleic palm oil via enzymatic acidolysis. J Teknol. **12**, 85–99 (2016)
14. Refaat, A.A.: Different techniques for the production of biodiesel from waste vegetable oil. Int J Environ Sci Tech. **7**, 183–213 (2010)
15. Phan, A.N., Phan, T.M.: Biodiesel production from waste cooking oils. Fuel. **87**, 3490–3496 (2008)
16. Corro, G., Tellez, N., Jimenez, T., Tapia, A., Banuelo, F., Vazquez-Cuchillo, O.: Biodiesel from waste frying oil. Two step process using acidified SiO_2 for esterification step. Catal Today. **166**, 116–122 (2011)
17. Lapuerta, M., Herreros, J.M., Lyons, L.L., Contreras, R.G., Briceño, Y.: Effect of the alcohol type used in the production of waste cooking oil biodiesel on diesel performance and emissions. Fuel. **87**, 3161–3169 (2008)
18. Mancini, A., Imperlini, E., Nigro, E., Montagnese, C., Daniele, A., Orrù, S., Buono, P.: Biological and nutritional properties of palm oil and palmitic acid: effects on health. Molecules. **20**, 17339–17361 (2015)
19. Meesuk, L., Seammai, S.: The use of perlite to remove dark colour from repeatedly used palm oil. Sci Asia. **36**, 33–39 (2010)
20. Fang, L., Yuan, W., Wang, B., Xiong, Y.: Growth of graphene on cu foils by microwave plasma chemical vapor deposition: the effect of in-situ hydrogen plasma post-treatment. Appl Surf Sci. **383**, 28–32 (2016)
21. Rajagopalan, B., Chung, J.S.: Reduced chemically modified graphene oxide for supercapacitor electrode. Nanoscale Res Lett. **9**, 1–10 (2014)

22. Aunkor, M.T.H., Mahbubul, I.M., Saidur, R., Metselaar, H.S.C.: The green reduction of graphene oxide. RSC Adv. **6**, 27807–27828 (2016)
23. Perumbilavil, S., Sankar, P., Priya Rose, T., Philip, R.: White light Z-scan measurements of ultrafast optical nonlinearity in reduced graphene oxide nanosheets in the 400–700 nm region. Appl Phys Lett. **107**, 051104 (2015)
24. Kudin, K.N., Ozbas, B., Schniepp, H.C., Prud'homme, R.K., Aksay, I.A., Car, R.: Raman spectra of graphite oxide and functionalized graphene sheets. Nano Lett. **8**, 36–41 (2007)
25. Calizo, I., Bejenari, I., Rahman, M., Liu, G., Balandin, A.A.: Ultraviolet raman microscopy of single and multilayer graphene. J Appl Phys. **106**, 043509 (2009)
26. Dong, X., Wang, P., Fang, W., Su, C.-Y., Chen, Y.-H., Li, L.-J., Huang, W., Chen, P.: Growth of large-sized graphene thin-films by liquid precursor-based chemical vapor deposition under atmospheric pressure. Carbon. **49**, 3672–3678 (2011)
27. Reina, A., Jia, X., Ho, J., Nezich, D., Son, H., Bulovic, V., Dresselhaus, M.S., Kong, J.: Large area, few-layer graphene films on arbitrary substrates by chemical vapor deposition. Nano Lett. **9**, 30–35 (2009)
28. Narula, U., Tan, C.M., Lai, C.S.: Growth mechanism for low temperature PVD graphene synthesis on copper using amorphous carbon. Sci Rep. **7**, 44112 (2017)
29. Lee, H.C., Liu, W.-W., Chai, S.-P., Mohamed, A.R., Lai, C.W., Khe, C.-S., Voon, C.H., Hashim, U., Hidayah, N.M.S.: Synthesis of single-layer graphene: a review of recent development. Procedia Chem. **19**, 916–921 (2016)
30. Nanda, S.S., Kim, M.J., Yeom, K.S., An, S.S.A., Ju, H., Yi, D.K.: Raman spectrum of graphene with its versatile future perspectives. TrAC Trends Anal Chem. **80**, 125–131 (2016)
31. Mishra, A.K., Ramaprabhu, S.: Carbon dioxide adsorption in graphene sheets. AIP Adv. **1**, 032152 (2011)
32. Jabbar, A., Yasin, G., Khan, W.Q., Anwar, M.Y., Korai, R.M., Nizam, M.N., Muhyodin, G.: Electrochemical deposition of nickel graphene composite coatings: effect of deposition temperature on its surface morphology and corrosion resistance. RSC Adv. **7**, 31100–31109 (2017)
33. Raghavan, N., Thangavel, S., Venugopal, G.: Enhanced photocatalytic degradation of methylene blue by reduced graphene-oxide/titanium dioxide/zinc oxide ternary nanocomposites. Mater Sci Semicond Process. **30**, 321–329 (2015)
34. Li, W.Z., Wen, J.G., Ren, Z.F.: Effect of temperature on growth and structure of carbon nanotubes by chemical vapor deposition. Appl Phys A Mater Sci Process. **74**, 397–402 (2002)
35. Chae, S.J., Güneş, F., Kim, K.K., Kim, E.S., Han, G.H., Kim, S.M., Shin, H.-J., Yoon, S.-M., Choi, J.-Y., Park, M.H., Yang, C.W., Pribat, D., Lee, Y.H.: Synthesis of large-area graphene layers on poly-nickel substrate by chemical vapor deposition: wrinkle formation. Adv Mater. **21**, 2328–2333 (2009)
36. Vinayan, B.P., Nagar, R., Ramaprabhu, S.: Solar light assisted green synthesis of palladium nanoparticle decorated nitrogen doped graphene for hydrogen storage application. J Mater Chem A. **1**, 11192–11199 (2013)
37. Liu, P., White, K.L., Sugiyama, H., Xi, J., Higuchi, T., Hoshino, T., Ishige, R., Jinnai, H., Takahara, A., Sue, H.-J.: Influence of trace amount of well-dispersed carbon nanotubes on structural development and tensile properties of polypropylene. Macromolecules. **46**, 463–473 (2013)
38. Gutierrez, G., Le Normand, F., Muller, D., Aweke, F., Speisser, C., Antoni, F., Le Gall, Y., Lee, C.S., Cojocaru, C.S.: Multi-layer graphene obtained by high temperature carbon implantation into nickel films. Carbon. **66**, 1–10 (2014)
39. Zhang, H., Feng, P.X.: Fabrication and characterization of few-layer graphene. Carbon. **48**, 359–364 (2010)
40. Song, X., Song, L., Chen, X., Zhang, T.: The characterization of graphene prepared using a nickel film catalyst pre-deposited to fused silica. RSC Adv. **6**, 22244–22249 (2016)
41. Ahmed, S.F., Khalid, M., Amin, N., Rashmi, W.: Investigation of rheological and corrosion properties of graphene-based eutectic salt. J Mater Sci. **53**, 692–707 (2018)
42. Kumar, M.K., Jha, N.S., Mohan, S., Jha, S.K.: Reduced graphene oxide-supported nickel oxide catalyst with improved CO tolerance for formic acid electrooxidation. Int J Hydrog Energy. **39**, 12572–12577 (2014)
43. Chaitoglou, S., Bertran, E.: Effect of temperature on graphene grown by chemical vapor deposition. J Mater Sci. **52**, 8348–8356 (2017)
44. Antony, R.P., Preethi, L.K., Gupta, B., Mathews, T., Dash, S., Tyagi, A.K.: Efficient electrocatalytic performance of thermally exfoliated reduced graphene oxide-Pt hybrid. Mater Res Bull. **70**, 60–67 (2015)
45. Jafari, A., Ghoranneviss, M., Gholami, M., Mostahsan, N.: The role of deposition temperature and catalyst thickness in graphene domains on cu. Int Nano Lett. **5**, 199–204 (2015)
46. Ghorannevis, Z., Jafari, A., Alipour, R., Ghoranneviss, M.: The effects of growth time on WO_3 nanostructure synthesized by HFCVD method. J Fusion Energ. **34**, 1157–1161 (2015)
47. Wu, C., Li, F., Chen, W., Veeramalai, C.P., Ooi, P.C., Guo, T.: Electromagnetic induction heating for single crystal graphene growth: morphology control by rapid heating and quenching. Sci Rep. **5**, 9034 (2015)
48. J.M. García, R. He, M.P. .Jiang, P. Kim, L.N. Pfeiffer and A. Pinczuk, "Multilayer graphene grown by precipitation upon cooling of nickel on diamond". Carbon, vol. 49, pp. 1006–1012, 2011
49. C.R. Woods, L. Britnell, A. Eckmann, R.S. Ma, J.C. Lu, H.M. Guo, X. Lin, G.L. Yu, Y. Cao, R.V. Gorbachev, A.V. Kretinin, J. Park, L.A. Ponomarenko, M.I. Katsnelson, Y.N. Gornostyrev, K. Watanabe, T. Taniguchi, C. Casiraghi, H-J. Gao, A. K. Geim and K.S. Novoselov, "Commensurate–incommensurate transition in graphene on hexagonal boron nitride". Nat Phys, vol. 10, pp. 451–456, 2014
50. Hong, R., Ji, J., Tao, C., Zhang, D., Zhang, D.: Fabrication of Au/graphene oxide/Ag sandwich structure thin film and its tunable energetics and tailorable optical properties. AIMS Mater Sci. **4**, 223–230 (2017)
51. Mennella, V., Colangeli, L., Bussoletti, E., Merluzzi, P., Monaco, G., Palumbo, P., Rotundi, A.: Laboratory experiments on cosmic dust analogues: the structure of small carbon grains. Planet Space Sci. **43**, 1217–1221 (1995)
52. Chen, Z., Zhang, N., Xu, Y.-J.: Synthesis of graphene–ZnO nanorod nanocomposites with improved photoactivity and anti-photocorrosion. CrystEngComm. **15**, 3022–3030 (2013)
53. Lai, Q., Zhu, S., Luo, X., Zou, M., Huang, S.: Ultraviolet-visible spectroscopy of graphene oxides. AIP Adv. **2**, 032146 (2012)
54. Mun, J.H., Hwang, C., Lim, S.K., Cho, B.J.: Optical reflectance measurement of large-scale graphene layers synthesized on nickel thin film by carbon segregation. Carbon. **48**, 447–451 (2010)
55. Russo, C., Stanzione, F., Alfè, M., Ciajolo, A., Tregrossi, A.: Spectral analysis in the UV-visible range for revealing the molecular form of combustion- generated carbonaceous species. Combust Sci Technol. **184**, 1219–1231 (2012)
56. Agorku, E.S., Mamo, M.A., Mamba, B.B., Pandey, A.C., Mishra, A.K.: Palladium-decorated zinc sulfide/reduced graphene oxide nanocomposites for enhanced visible light-driven photodegradation of indigo carmine. Mater Sci Semicond Process. **33**, 119–126 (2015)